Crystal Structure of Pyranose 2-Oxidase from the White-Rot Fungus *Peniophora* sp.[†,‡]

Michael Bannwarth,[§] Sabine Bastian,[||] Dorothee Heckmann-Pohl,[||] Friedrich Giffhorn,[||] and Georg E. Schulz*[,§]

Institut für Organische Chemie und Biochemie, Albert-Ludwigs-Universität, Albertstrasse 21, 79104 Freiburg im Breisgau, Germany, and Lehrstuhl für Angewandte Mikrobiologie, Universität des Saarlandes, Im Stadtwald, Gebäude 2, 66123 Saarbrücken, Germany

Received July 1, 2004; Revised Manuscript Received July 22, 2004

ABSTRACT: Pyranose 2-oxidase catalyzes the oxidation of a number of carbohydrates using dioxygen. The enzyme forms a D_2 symmetric homotetramer and contains one covalently bound FAD per subunit. The structure of the enzyme from *Peniophora* sp. was determined by multiwavelength anomalous diffraction (MAD) based on 96 selenium sites per crystallographic asymmetric unit and subsequently refined to good-quality indices. According to its chain fold, the enzyme belongs to the large glutathione reductase family and, in a more narrow sense, to the glucose−methanol−choline oxidoreductase (GMC) family. The tetramer contains a spacious central cavity from which the substrate enters one of the four active centers by penetrating a mobile barrier. Since this cavity can only be accessed by glucose-sized molecules, the enzyme does not convert sugars that are part of a larger molecule. The geometry of the active center and a comparison with an inhibitor complex of the homologous enzyme cellobiose dehydrogenase allow the modeling of the reaction at a high confidence level.

Pyranose 2-oxidase (P2ox,[1] pyranose:oxygen 2-oxidoreductase, EC 1.1.3.10) is presumably located in the hyphal periplasmic space, an outer compartment of the fungal hyphae (*1*). It produces hydrogen peroxide from molecular dioxygen by dehydrogenating a range of carbohydrates. The hydrogen peroxide is then used by lignin peroxidases for degrading lignin and thus wood (*2*). The enzyme was isolated from numerous white-rot fungi (*3*−*7*), in some of which P2ox produces most of the hydrogen peroxide required for wood degradation. In others, the second P2ox reaction product 2-ketoglucose is further metabolized to the antibiotic cortalcerone which protects the fungus from bacterial attack (*8*). In *Tricholoma matsutake*, P2ox was identified as the main carrier of a strong antifungal activity which is based on an unidentified P2ox reaction product (*9*).

The P2ox reaction can be divided into two steps: the oxidation of the carbohydrate by FAD and the regeneration of reduced FAD by dioxygen (Figure 1). Interestingly, the regeneration of reduced FAD can also be achieved by benzoquinones and related substances produced during lignin degradation (*10*). The substrate specificity of the enzyme is rather broad: D-glucose, D-xylose, and L-sorbose are oxidized at high rates and many other carbohydrates at slower rates (*11*). P2ox is the only enzyme that oxidizes pyranoses at the C2 position. Since P2ox shows no anomer preference and a higher affinity for D-glucose (*1*) than glucose oxidase, it may in future replace the latter in clinical diagnostics. For applications, it is most convenient that the fungal enzymes can be expressed in *Escherichia coli*. Cytosolic expression yielded active P2ox from *Coriolus versicolor* (*6*) and *Trametes ochracea* (*7*) as well as an inactive enzyme from *T. matsutake* (*9*).

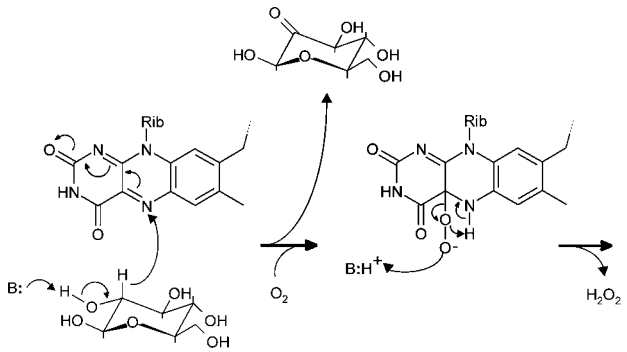

FIGURE 1: Expected reaction scheme of the 2-oxidation of glucose in P2ox. A hydride ion is transferred to the N5 atom of the isoalloxazine to form an $FADH^-$ intermediate, which is then regenerated to FAD by dioxygen.

On the basis of sequence comparisons, it was suggested that P2ox belongs to the GMC family of enzymes (*12*). This family was originally defined on the basis of sequences (*13*). Now it is supported by the structures of four family members, namely, cholesterol oxidase (*14*−*16*), glucose oxidase (*17*, *18*), hydroxynitrile lyase (*19*), and cellobiose dehydrogenase (*20*). Among them, the latter is most closely related to P2ox, being 19% identical in a sequence-based alignment. In a

[†] This work was supported by the Deutsche Forschungsgemeinschaft under Grant SFB-388.

[‡] The atomic coordinates and structure factors are deposited in the Protein Data Bank as entry 1TZL.

* To whom correspondence should be addressed: Institut für Organische Chemie und Biochemie, Albertstr. 21, D-79104 Freiburg, Germany. Telephone: +49-761-203-6058. Fax: +49-761-203-6161. E-mail: georg.schulz@ocbc.uni-freiburg.de.

[§] Albert-Ludwigs-Universität.

[||] Universität des Saarlandes.

[1] Abbreviations: GMC family, glucose−methanol−choline family; MAD, multiwavelength anomalous diffraction; P2ox, pyranose 2-oxidase.

10.1021/bi048609q CCC: $27.50
Published on Web 08/27/2004

broader comparison, the chain folds of the GMC family members constitute a subgroup of the glutathione reductase family (*21*, *22*) and, in particular, of glutathione reductase family 2 (*22*). Here, we report the structure of the enzyme P2ox from *Peniophora* sp., show that it is a member of the GMC family, and propose the geometry of the catalyzed reaction.

MATERIALS AND METHODS

Production and Purification of SeMet-Labeled P2ox. Full-length P2ox (GenBank accession number AF535193) was produced in methionine auxotrophic *E. coli* strain B834(DE3) (Novagen) using pET-24a(+) (Novagen) as the expression vector. The bacteria were grown overnight at 37 °C in 2 mL of Luria-Bertani broth, harvested by centrifugation (2500*g* for 5 min), resuspended in 100 mL of LeMaster medium (*23*), and grown overnight at 37 °C. Subsequently, they were cultivated in 1000 mL of LeMaster medium up to an OD_{600} of 1.0. P2ox expression was then induced by adding 0.1 mM isopropyl β-D-thiogalactopyranoside (IPTG), and growth was continued for an additional 48 h at 20 °C. All subsequent handling was carried out at 4 °C.

Harvested wet cells (12 g) were resuspended in 50 mL of 100 mM potassium phosphate (pH 7.0) and sonicated five times for 15 s. Cell debris was separated by centrifugation (23000*g* for 30 min). Ammonium sulfate was added to 40% saturation, and the precipitate was removed by centrifugation. The supernatant was applied to a Phenyl-Sepharose column (116 mm × 16 mm) equilibrated with 40% saturated ammonium sulfate in 50 mM potassium phosphate (pH 7.0). P2ox was then eluted with the same buffer without ammonium sulfate. The collected P2ox fractions were concentrated by ultrafiltration and passed through a Sephacryl S-300 column (890 mm × 26 mm) equilibrated with 50 mM Bis-Tris (pH 6.4). The P2ox fractions were adjusted to pH 7.2 and applied to a Q-Sepharose Fast Flow column (90 mm × 26 mm) equilibrated with 25 mM sodium acetate (pH 7.2). P2ox eluted at 400 mM as part of a linear gradient from 25 to 1000 mM sodium acetate (pH 7.2) and was adjusted to 100 mM sodium acetate (pH 7.2), concentrated by ultrafiltration, and stored.

Crystallization and X-ray Data Collection. The protein was further purified by gel-permeation chromatography (640 mm × 15 mm Fractogel, Novagen), concentrated by ultrafiltration, dialyzed against 1 mM DTT, and crystallized in hanging drops containing 2 μL of a 7 mg/mL protein solution and 2 μL of reservoir buffer [19% PEG-6000 in 100 mM MES (pH 6.0)] at 20 °C. To prevent selenium oxidation, the reservoir contained in addition 150 mM tributylphosphine (not dissolved). The crystals grew within 2 weeks to dimensions of ~180 μm × ~120 μm × ~80 μm. One crystal was transferred in three steps to a cryo solution containing 30% PEG-6000, 15% 2-methyl-2,4-pentanediol, and 10 mM tributylphosphine (not dissolved) in 100 mM MES (pH 6.0) and then flash-frozen in a 100 K nitrogen gas stream. Multiwavelength anomalous diffraction (MAD) data were collected at beamline X06SA-PX of the Swiss Light Source (Villigen, Switzerland) using a CCD detector (Marresearch).

Data Processing and Structure Analysis. The diffraction images were processed using XDS (*24*). Selenium sites were established with SHELXD (*25*) using single-wavelength anomalous difference Patterson maps. On the basis of the SHELXD result, 96 sites with an occupancy of >0.4 were selected, and the correct hand of the selenium substructure was derived from an electron density map produced with SHELXE (*26*). The selenium sites were subsequently refined, and phases were calculated with MLPHARE (*27*), SOLVE (*28*), and SHARP (*29*). The resulting electron density allowed automatic building of part of the model with RESOLVE (*28*). The remainder of the model was added manually using O (*30*). The model coordinates were refined with CNS (*31*) and REFMAC (*32*). The FAD library files were generated using PRODRG (*33*) and REFMAC. The refinement started with noncrystallographic symmetry (NCS) restraints, which were later relaxed and eventually completely removed. Water molecules were established with ARP/wARP (*34*) and with REFMAC. Figures were produced using POVSCRIPT+ (*35*) and MSMS (*36*).

Table 1: Data Collection and Refinement Statistics[a]

	Data Collection		
	peak	inflection	remote
wavelength (Å)	0.97934	0.97950	0.93926
resolution (Å)	20−2.35	20−2.44	20−2.66
no. of observations	859625	766811	598549
no. of unique reflections	432664	387797	301803
completeness (%)	96 (95)	96 (94)	97 (96)
$R_{sym\ I}$ (%)	6.6 (21)	6.8 (23)	7.2 (23)
multiplicity	2.0 (2.0)	2.0 (2.0)	2.0 (2.0)
average I/σ_I	8.4 (4.0)	8.1 (3.9)	8.4 (4.0)

Refinement	
resolution range (Å), no. of reflections	19.7−2.35, 219141
no. of protein atoms, FAD atoms, water molecules	36400, 424, 2154
average *B*-factors (Å^2; main chain, side chains, FAD)	18, 20, 17
rmsd for bond lengths (Å), bond angles (deg)	0.017, 1.45
R_{cryst} (%), R_{free} (%)	17.6, 22.6
Ramachandran plot (%; most favored, other)	88, 12[b]

[a] All data collection was carried out at 100 K. The numbers in parentheses refer to the last shell. The crystal belonged to space group $P2_1$ with two tetramers per crystallographic asymmetric unit with the following cell dimensions: $a = 164.9$ Å, $b = 103.6$ Å, $c = 169.2$ Å, and $\beta = 105.3°$. [b] Mostly in additionally allowed but 0.1% in generously allowed regions. Pro266 forms a *cis*-peptide bond.

RESULTS AND DISCUSSION

Crystal Structure of P2ox. P2ox from *Peniophora* sp. is a homotetramer of four chains of 623 amino acid residues and four covalently attached FAD molecules. The structure of the selenomethionine-labeled enzyme was determined with the MAD method. The resolution dropped from 2.35 to 2.66 Å during data collection (Table 1). The crystals were expected to contain two tetramers per asymmetric unit because the corresponding packing density of 2.6 Å^3/Da is in the usual range. Using the data set collected at the peak of the selenium absorption and an anomalous difference Patterson map, a total of 96 selenium sites were assigned. This number corresponds to 75% of the 16 methionines per subunit (without the N-terminal residue). The phases were calculated using the MAD method. The resulting electron density map revealed the two expected P2ox tetramers in the crystallographical asymmetric unit. For the refinement, we used the highest-resolution data set (Table 1). The refined model consisted of 4616 amino acid residues and eight FAD molecules. Moreover, it included 0.47 water molecule per amino acid residue which is appropriate at 2.35 Å resolution.

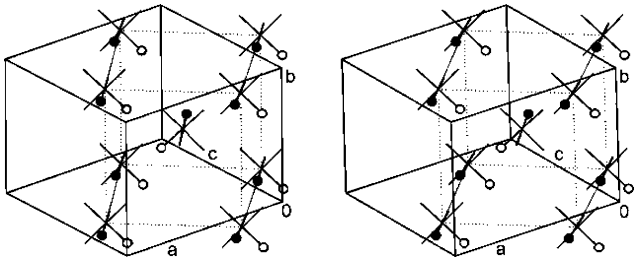

FIGURE 2: Packing of D_2 symmetric P2ox tetramers in the crystal with space group $P2_1$ showing the outline of the unit cell (Table 1). The three molecular axes are distinguished from each other by markers. The asymmetric unit contains the two tetramers in the a−c plane. The 2_1 axis is vertical. If small rotational and translational displacements are neglected, the packing converts to a halved unit cell marked by dotted lines. This pseudo-unit cell belongs to space group $P4_22_12$ with one subunit of the tetrameric P2ox in the asymmetric unit. The pseudo-4_2 axis points toward the reader. It explains the 4-fold axis observed in the self-rotation function.

The quality indices were in a favorable range. The model was further confirmed as all selenium sites were located at methionines.

Since large asymmetric units are likely to contain *pseudo*-symmetric packings (*37*), we analyzed the arrangement of the tetramers neglecting the actual unit cell and the actual space group $P2_1$. This revealed a packing close to space group $P4_22_12$ with unit cell axes of 101 Å × 104 Å × 133 Å and one subunit in the asymmetric unit (Figure 2). The deviations from this highly symmetric packing scheme were merely a tilt of a couple of degrees and a displacement of a couple of angstroms. This explained why the self-rotation function showed a single very strong peak at $\kappa = 90°$ pointing to a local 4-fold axis, although the D_2 symmetric tetramers contain only 2-fold axes.

The P2ox tetramer has dimensions of ~90 Å × ~90 Å × ~130 Å in accordance with electron microscopy estimates (*5*, *10*). The interfaces between the subunits in the tetramer are 470 (A−B), 2600 (A−C), and 1130 Å^2 (A−D), adding up to 4200 Å^2, which is 16% of the solvent-accessible surface of an isolated subunit of 25 500 Å^2. All crystal packing contacts between tetramers were below 430 Å^2 so that the assignment of the tetramers was clear. All eight subunits in the asymmetric unit are structurally very similar, showing an rmsd of 0.3 Å in binary Cα comparisons. The maximum deviation was 2.8 Å. The *B*-factor distribution of one subunit and the sequence of P2ox are shown in Figure 3. The other seven subunits have almost identical distributions, and the overall rmsd amounts to merely 1.6 Å^2. Therefore, we conclude that the deviations at packing contacts are very small. The enzyme contains an FAD molecule covalently linked with its 8-methyl group to His167 Nε2. This is a common linkage type and also confirms previously published data (*38*, *39*). The *B*-factors of FAD match those of the surrounding peptide, indicating full occupancy. The covalent attachment allows P2ox to survive in an extracellular environment where noncovalently bound cofactors tend to disappear via diffusion. The chain fold and the surface structures of P2ox are shown in Figure 4.

P2ox Enzyme Family. A data bank search with BLAST (*40*) revealed a total of nine P2ox sequences that were separated from all others by a sharp drop in the degree of sequence similarity. Further comparisons within this group showed a very close relationship between the enzymes from *Peniophora* sp., *Tr. ochracea*, and *C. versicolor* (all comparisons show >95% identical residues) and between the enzymes from *Trametes hirsuta* and *Phlebiopsis gigantea* (97% identical), which are therefore represented by only one species each in Table 2. All species align over their whole length and are more than 34% identical with each other, indicating that their structures are closely related. The included hypothetical protein from *Aspergillus nidulans* is

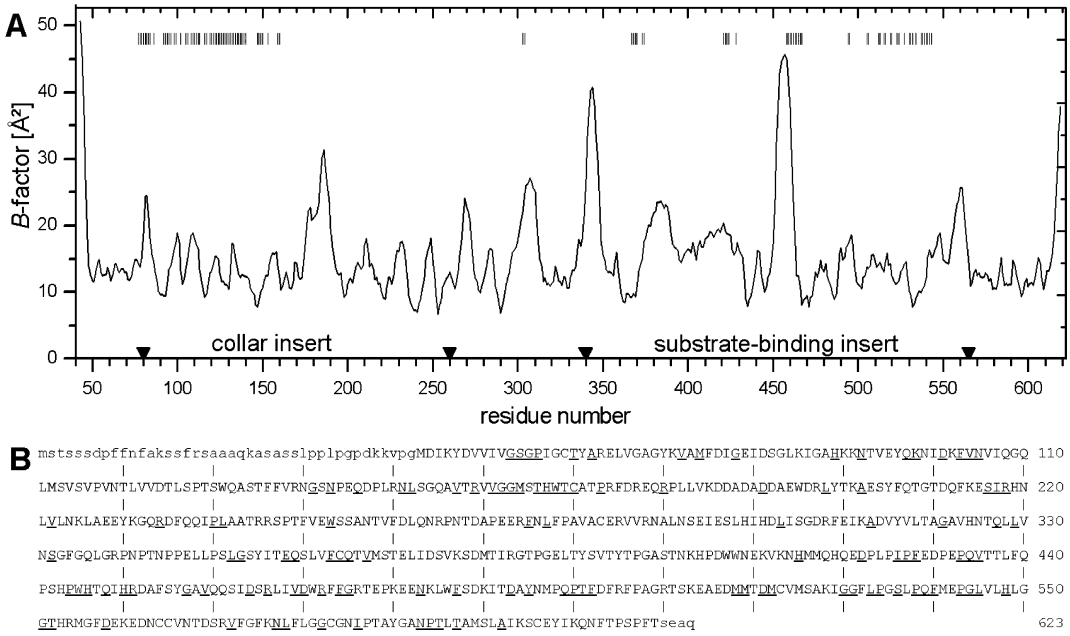

FIGURE 3: Polypeptide chain of P2ox from *Peniophora* sp. (A) *B*-factor distribution of subunit A. The distributions of the other seven subunits in the crystallographic asymmetric unit are almost identical. The residues at the tetramer interfaces are indicated in the top line. The A−B contact involves residues of the 516−539 segment and the A−D contact residues of 122−159 and 505−543 segments. The A−C contact residues are scattered over the range of residues 70−540. (B) Sequence of P2ox from *Peniophora* sp. (see Materials and Methods). The unstructured N- and C-terminal segments are denoted with lowercase letters. The strictly conserved residues of the P2ox family are underlined.

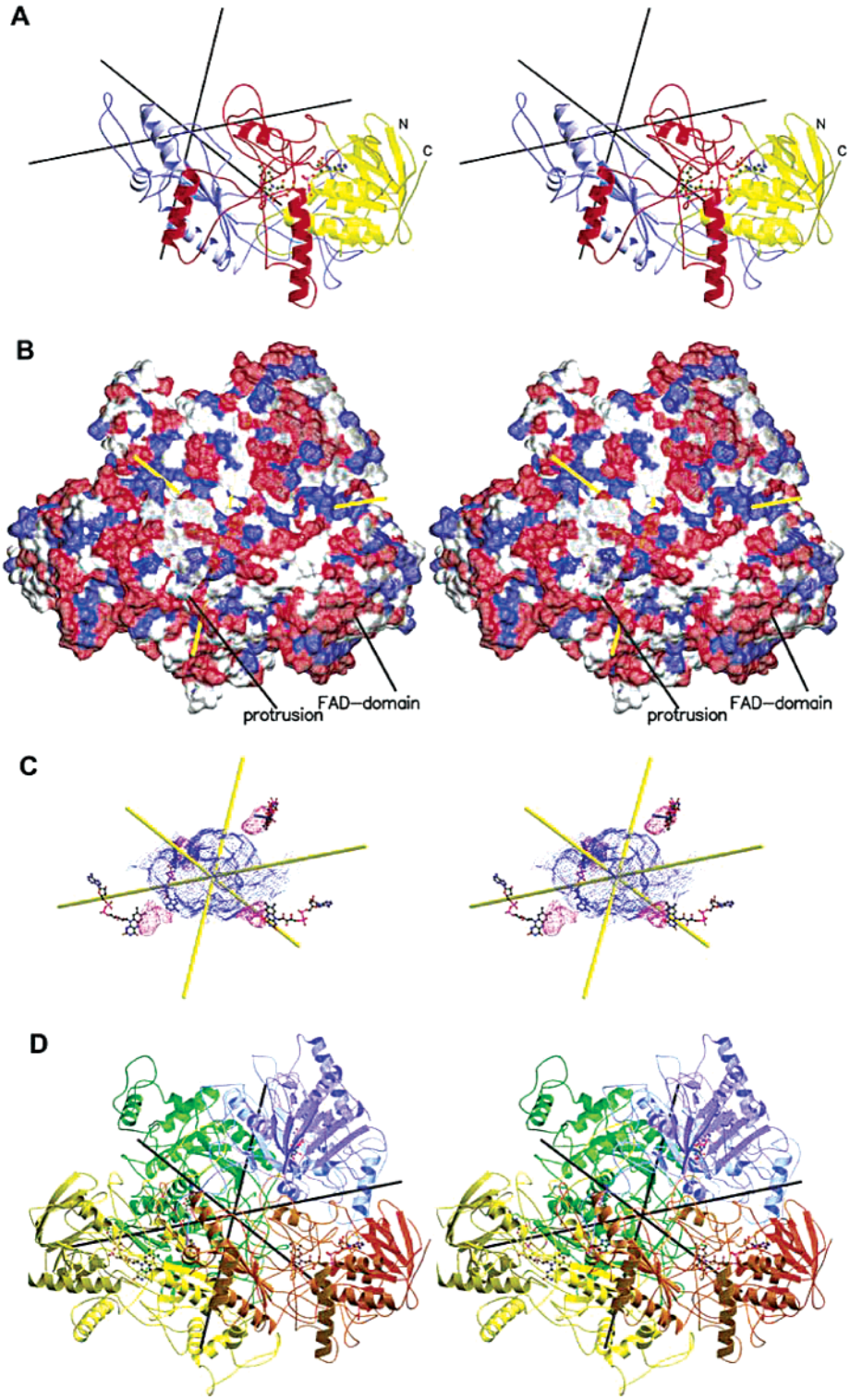

FIGURE 4: Structure of P2ox from *Peniophora* sp. (A) Ribbon plot of one subunit. The FAD domain is yellow, the collar insert red, and the substrate-binding insert blue. The FAD molecule is depicted in a ball-and-stick representation. The symmetry axes are shown. The depicted secondary structures correspond to those of Figure 5. Several small secondary structure segments are ignored for the sake of clarity. (B) Surface representation of the P2ox tetramer with symmetry axes. The view is into one of the four entrances to the central cavity from where all four active centers can be accessed. The entrance is located in the largest tetramer interface between subunits A and C. The protruding FAD domain and the P2ox protrusion of residues 372−427 are marked. The colors show positively (blue) and negatively (red) charged residues. (C) Surface of the central inner cavity (blue) and of the substrate-binding pockets (red) at the *re*-faces of the four isoalloxazines. The entrance to the cavity is visible. (D) Ribbon plot of the tetramer in the same orientation and with the same secondary structures described above. The subunit colors are yellow (A), orange (B), green (C), and blue (D).

most likely a P2ox because it is well-embedded in the P2ox family (Table 2). We therefore conclude that the reported structure of P2ox from *Peniophora* sp. represents these enzymes with reasonable accuracy. The residues conserved throughout the P2ox family are marked in the sequence given in Figure 3B. They comprise the flavin attachment region around position 167 and the active center around position 548. It was suggested that the 28 N-terminal residues of P2ox

Table 2: Sequence Comparisons within the P2ox Family[a]

	PENSP	TRAHI	LYSHI	PHACH	ASNID	TRIMA
PENSP	–	83	45	41	37	35
TRAHI		–	45	41	38	35
LYSHI			–	54	39	41
PHACH				–	37	37
ASNID					–	36

[a] All values denote percent identical residues related to the average length of the two compared chains. Abbreviations: PENSP, *Peniophora* sp. (close to *Tr. ochracea* and *C. versicolor*); TRAHI, *Tr. hirsuta* (close to *P. gigantea*); LYSHI, *Lyophyllum shimeji*; PHACH, *Phanerochaete chrysosporium*; ASNID, *A. nidulans* (hypothetical protein); TRIMA, *T. matsutake*.

Table 3: Structural Comparisons within the GMC Family Using DALI (*42*)[a]

	Gox	HNL	CbDH	Chox	P2ox
Gox	–	85.0 (35.2)	80.5 (31.8)	73.7 (25.8)	71.5 (25.9)
HNL		–	81.4 (34.2)	78.1 (28.8)	76.1 (28.0)
CbDH			–	79.3 (29.0)	72.6 (30.1)
Chox				–	75.7 (27.5)

[a] Given are the percentages of aligned residues related to the average lengths of the structured chain together with the respective *Z*-scores in parentheses. The Cα atoms of aligned residues are closer than 3.0 Å. Abbreviations (structured chain lengths): Gox (587), glucose oxidase (*18*); HNL (521), hydroxynitrile lyase (*19*); CbDH (541, omitting the unrelated cytochrome domain), cellobiose dehydrogenase (*20*); Chox (498), cholesterol oxidase (*16*); P2ox (577), reported enzyme.

target this enzyme to the hyphal periplasmic space, like lignin peroxidase (*6*). However, the putative signal peptide was not recognized with SIGNALP trained with eukaryotic sequences (*41*), but it was detected with SIGNALP trained with sequences from either Gram-positive or Gram-negative bacteria. In our crystal, this part of the polypeptide has no structure (Figure 3B), which is consistent with the signal peptide hypothesis.

P2ox as a Member of the GMC Family. Flavoenzymes have been subdivided into several families, among them the GMC family of enzymes (*13*) as part of broader glutathione reductase family 2 (*22*). To confirm the sequence-based assignment of P2ox to the GMC family (*12*), we performed a structure data bank search using DALI (*42*). This revealed the four structurally established GMC family members (*14*−*20*) with *Z*-scores ranging from 30.1 to 25.9 as close structural relatives that were well-separated from all others. The other structures showed *Z*-scores of ≤17.2; those of other flavoenzymes ranged between 17 and 10, with glutathione reductase having a *Z*-score of 11.

Structural comparisons within the GMC family are reported in Table 3. They indicate close relationships between glucose oxidase, hydroxynitrile lyase, and cellobiose dehydrogenase forming a cluster. Cholesterol oxidase and P2ox are successively further apart from this cluster. However, the structural relationship is rather close because more than 70% of all residues can be aligned within the usual 3 Å cutoff for Cα atoms. Each of the five chain folds shows some specific insertions when compared with all others. The specific insertions of P2ox are residues 115−148 which form a long loop embracing another subunit of the tetramer, and residues 372−427 forming a protrusion of the structure (Figure 4). A smaller protrusion with a different structure at this position is also present in cellobiose dehydrogenase. Both

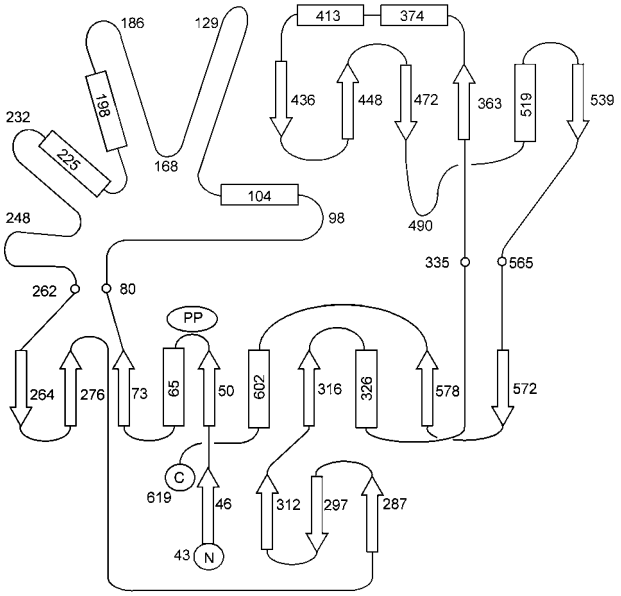

FIGURE 5: Chain fold topology plot of P2ox referenced to the greater glutathione reductase family. The α-helices are represented by rectangles and the β-strands by arrows. Several small secondary structures have been omitted for clarity. Both are labeled using internal residue numbers. All connections between parallel β-strands are right-handed as usual. Accordingly, β-sheet-46-312-297-287 and α-helix-326 are in front of β-sheet-264-276-73-50-316-578-572, whereas α-helices-65 and -602 are at the rear side. The borders to the collar insert (left) and to the substrate-binding insert (right) are depicted. Residue numbers at the apexes of loops are given. Note that the inserts are larger than the FAD domain that is used as the reference.

enzymes use degradation products of wood as substrates so that the protuberance may play a role in the natural environment.

Within the GMC family, hydroxynitrile lyase, cellobiose dehydrogenase, and cholesterol oxidase are monomeric, while glucose oxidase is a dimer and P2ox a tetramer. The dimer of glucose oxidase corresponds clearly to the putative dimer of subunits A and C of P2ox, which has by far the largest area among the three interfaces in the tetramer (see above). However, this interface is not very strongly conserved, giving rise to deviations in the range of 10 Å between the respective dimers.

Chain Fold Topology of P2ox. The chain fold of P2ox is essentially the same as those of the other members of the GMC family (Figure 4). Interestingly, this chain fold cannot be subdivided into sequential compact domains as in most other proteins of this size, making a simple description impossible. Therefore, we use the presumed evolutionary connection of the GMC family to the more general glutathione reductase family (*22*) and describe P2ox in terms of the more general family (Figure 5). The central part of the chain fold of the glutathione reductase family is the five-stranded parallel β-sheet that binds FAD in a common geometry (*21*, *43*) with the pyrophosphoryl group at the loop between the first β-strand and the following α-helix and the adenine ribose at the end of the second β-strand of the reference β-sheet. If the connections between β-strands are included, this part is usually called the FAD domain. In P2ox, this reference is β-sheet-276-73-50-316-578 that binds FAD in the same manner as the whole greater family. Here, the β-strands are named after the positions of middle residues.

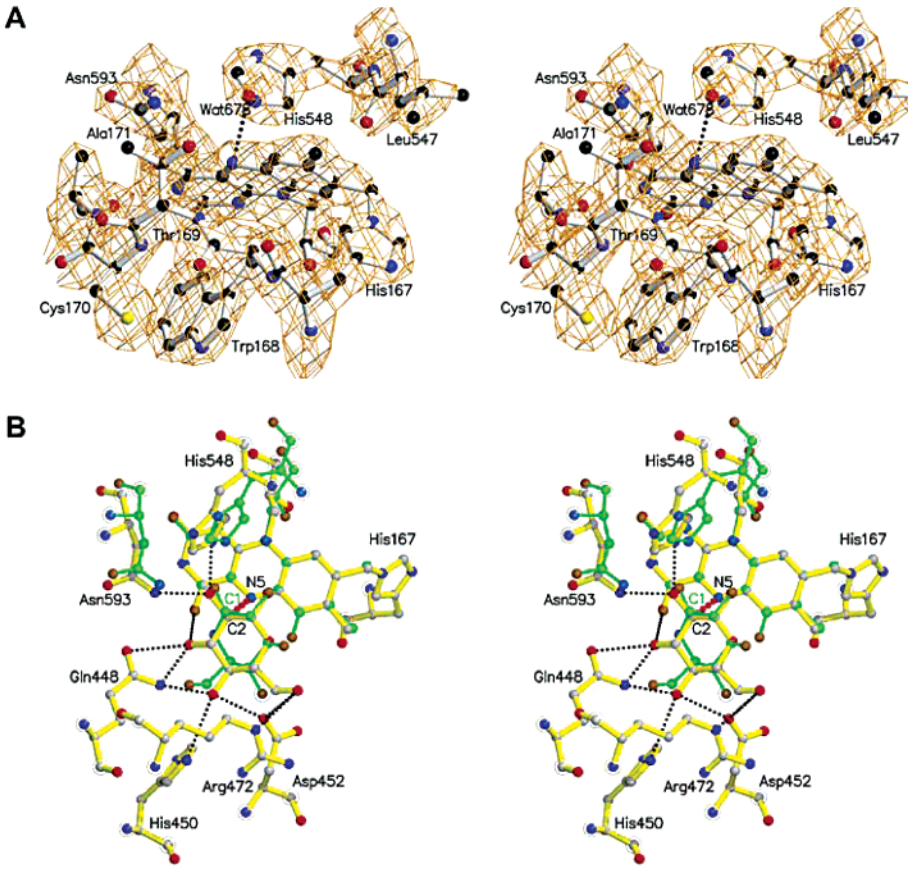

FIGURE 6: Catalytic center and reaction. (A) The $2F_o - F_c$ density contoured at 1.5σ around the flavin. Residues 167−171 at the *si*-side of the isoalloxazine are unique for P2ox when compared with those of the GMC family. The isoalloxazine is slightly bent. Electron density for the covalent bond and electron density for the active center water molecule Wat678 are clearly visible. (B) Superposition of the isoalloxazine ring of P2ox with the 6-hydroxyisoalloxazine of cellobiose dehydrogenase (green, noncovalently bound). The bound inhibitor cellobionolactam of the dehydrogenase is shown (green). A glucose molecule was modeled at the inhibitor position and perfectly explains the reaction by a hydride transfer to the N5 atom (dotted line). Only the P2ox residues are labeled. Wat678 is essentially at the C2 atom of the glucose model.

The labeled residues are also in one hydrogen bonding line. As in the glutathione reductase family, the third strand (β-strand-276) of this sheet is connected through a β-meander (antiparallel β-sheet-312-297-287) with the fourth strand (β-strand-316). The other antiparallel strands (β-strands-46, -264, and -572) constitute small additions at the edges of the central construction that are special for P2ox.

Using the FAD domain as the reference, P2ox shows two large insertions, one after the second and one after the fourth central parallel β-strand. Most interestingly, the 162-residue insertion after the second strand (β-strand-73) of P2ox corresponds to a 60-residue insertion of glutathione reductase that is probably involved in enzyme regulation (*21*). Furthermore, the 230-residue insertion after the fourth strand (β-strand-316) and the following helix (α-helix-326, named after a residue position in the middle) is inserted at the same position as the 140-residue NADP domain of glutathione reductase. The first P2ox insert after β-strand-73 assumes a scattered nonglobular structure (Figure 4) that is here considered a collar of several loops sitting on the FAD domain rump and therefore named "collar insert". The five loops are dispersed over the whole chain fold and cannot be considered a domain. The second P2ox insertion contains a compact part around antiparallel β-sheet-436-448-472-363-539 (Figures 4 and 5) but is elongated over 90 Å, forming numerous interactions with other parts of the enzyme. Consequently, it cannot be considered a domain like the corresponding insert of glutathione reductase. Since this insertion binds the substrate, it has been named the "substrate-binding insert". Both insertions contain further small two-stranded β-sheets and short α- and 3_{10}-helices that have been ignored for the sake of clarity in Figures 4 and 5. We therefore conclude that P2ox together with the whole GMC family is a derivative of a primordial FAD-binding domain that developed large insertions at the same positions as glutathione reductase and numerous other members of this large family (*22*).

Active Center and Catalytic Mechanism. Because of the oxidase activity of P2ox, the active center is presumably located at the isoalloxazine of FAD. Like in the other GMC enzymes and also in the greater glutathione reductase family, the *si*-face of isoalloxazine is covered by the peptide chain. In P2ox, the respective chain segment follows His167 of the collar insert that binds FAD covalently. The *si*-face residues of P2ox differ from those of other GMC family members. In particular, Trp168 conserved in all P2ox sequences (Figure 3B) replaces an Asn or His found in all other GMC members (*20*). Trp168 makes an edge-on contact with the isoalloxazine (Figure 6A). Due to the conformational change between oxidized and reduced isoalloxazine, Trp168 may therefore increase the oxidation potential of FAD as it may press on the isoalloxazine stabilizing the bent reduced form. A further

increase may come from the interaction between the indol aromatic edge hydrogens and the π-electrons of the isoalloxazine (*44*). Moreover, the oxidation potential may be increased by the covalent attachment of FAD to His167, as demonstrated for a similar attachment in vanillyl alcohol oxidase (*45*). Unfortunately, the redox potential of P2ox has not yet been determined.

The *re*-face of the isoalloxazine opposes His548 of the substrate-binding insert which is strictly conserved throughout the GMC family (*12*), acting most likely as a catalytic base in all of them (*17*). The active center location at the *re*-face is conserved in most enzymes of the broad glutathione reductase family (*21*, *22*). In the reported P2ox structure, it contains no substrate but only a water molecule (Wat678 in subunit A) that forms a short hydrogen bond with the N5 atom of the isoalloxazine. However, the structure of the homologous GMC family member cellobiose dehydrogenase contained the inhibitor cellobiono-1,5-lactam (*46*) and therefore revealed the putative glucose position in P2ox through a structural comparison (Figure 6B).

In numerous enzymes, the access of substrate to the active center is restricted. In some GMC enzymes, a so-called "loop-and-lid" structure has been assigned to this task (*20*). In P2ox, however, the corresponding chain segment is unlikely to limit substrate access to the active center. An accessible surface calculation revealed one large cavity at the center of the P2ox tetramer and four smaller pockets at the *re*-faces of the isoalloxazines (Figure 4C) that can only be entered from the central cavity and only by a rearrangement of the highly mobile loop of residues 453−460 and in particular by a conformational change that removes the side chain of Phe454. On the other hand, a glucose molecule can only reach the central cavity by passing through a small pore lined by residues Ile100, Pro248, Glu429, and Ser465 of subunit A and Asn140 and Ala494 of subunit C (Figure 4B). A second channel connecting the outside with the central cavity of the tetramer is at Thr120, which is at the 2-fold axis relating subunits A and D to each other. However, this channel is not large enough for a glucose, although appropriate for the second substrate dioxygen. This extreme shielding of the active center prevents P2ox from destroying pyranoses of glycoproteins, lipids, and the cell wall sugar chains.

Within the central cavity, residues Ile107, Leu111, Phe454, Phe474, Met541, and Leu547 may form a pathway for the movement of pyranose to the active center by providing favorable nonpolar contacts to the sugar top and bottom faces (*44*, *47*). Such weak binding helps the pyranose follow the rather long migration path of the pyranoses to the active center and back.

A model of the Michaelis complex of P2ox is shown in Figure 6B. It was derived from a superposition of the homologous cellobiose dehydrogenase with the bound inhibitor cellobionolactam. The glucose model was placed at the superimposed inhibitor so that its 2-hydroxyl fits O1 of cellobionolactam and also forms hydrogen bonds with His548 Nϵ2 and Asn593 Nδ1. The latter stabilizes the ketone. At this location, the H2 of the glucose points directly to the N5 atom of isoalloxazine so that the two electrons can be easily transferred via a hydride ion. A concomitant protonation of the base His458 yields the 2-keto sugar (Figure 1). The reduced isoalloxazine is stabilized by its environment (see above). After the 2-keto sugar has left the active center, the reduced isoalloxazine is then reoxidized by dioxygen or by other oxidizing mediators that can reach it, i.e., that are the same size as a pyranose.

Comparing the cellobiose dehydrogenase−inhibitor complex with the glucose model in P2ox (Figure 6B), we observe that His548 Nϵ2 of P2ox binds the 2-hydroxyl group and is displaced by 0.7 Å with respect to its position in the homologue where it binds the 1-hydroxyl group. Note that in P2ox the β-face of the pyranose model contacts the isoalloxazine in contrast to the homologous inhibitor that orients its α-face toward isoalloxazine. In the case of the slow pyranose C3 oxidation side reaction of P2ox (*11*), though, the orientation of the substrate is most likely that of cellobionolactam because this is the only way to bring the hydrogen atom at the pyranose C3 position to the N5 atom of the FAD.

Conclusion. The structure of P2ox from *Peniophora* sp. is representative of the whole P2ox family. Moreover, P2ox shares a common chain fold with the structurally established GMC oxidoreductases, which classifies P2ox as a family member despite its low level of sequence similarity. The tetrameric structure of the enzyme is unique in the GMC family. The tetramer forms a central cavity that can be accessed only through four glucose-sized pores. Moreover, the active center is protected by a highly mobile peptide from immediate access from the central cavity which differs from the loop-and-lid segment of other GMC family members. Consequently, P2ox restricts access to the active center drastically, thus preventing oxidation of macromolecular sugars. The catalytic base of P2ox, His548, is conserved across the whole GMC family, whereas the peptide sequence at the *si*-face of the isoalloxazine of FAD is a specialty of P2ox.

ACKNOWLEDGMENT

We thank the team of the Swiss Light Source for help in data collection and C. Schleberger and D. Kloer for help in data processing.

REFERENCES

1. Giffhorn, F. (2000) Fungal pyranose oxidases: occurrence, properties and biotechnical applications in carbohydrate chemistry, *Appl. Microbiol. Biotechnol. 54*, 727−740.
2. ten Have, R., and Teunissen, P. J. M. (2001) Oxidative mechanisms involved in lignin degradation by white-rot fungi, *Chem. Rev. 101*, 3397−3413.
3. Janssen, F. W., and Ruelius, H. W. (1975) Pyranose oxidase from *Polyporus obtusus*, *Methods Enzymol. 41*, 170−173.
4. Danneel, H. J., Rössner, E., Zeeck, A., and Giffhorn F. (1993) Purification and characterization of a pyranose oxidase from the basidiomycete *Peniophora gigantea* and chemical analyses of its reaction products, *Eur. J. Biochem. 214*, 795−802.
5. Schäfer, A., Bieg, S., Huwig, A., Kohring, G. W., and Giffhorn, F. (1996) Purification by immunoaffinity chromatography, characterization, and structural analysis of a thermostable pyranose oxidase from the white rot fungus *Phlebiopsis gigantea*, *Appl. Environ. Microbiol. 62*, 2586−2592.
6. Nishimura, I., Okada, K., and Koyama, Y. (1996) Cloning and expression of pyranose oxidase cDNA from *Coriolus versicolor* in *Escherichia coli*, *J. Biotechnol. 52*, 11−20.
7. Vecerek, B., Maresova, H., Kocanova, M., and Kyslik, P. (2004) Molecular cloning and expression of the pyranose 2-oxidase cDNA from *Trametes ochracea* MB49 in *Escherichia coli*, *Appl. Microbiol. Biotechnol. 64*, 525−530.
8. Koths, K., Halenbeck, R., and Moreland, M. (1992) Synthesis of the antibiotic cortalcerone from D-glucose using pyranose 2-oxi-

dase and a novel fungal enzyme, aldos-2-ulose dehydratase, *Carbohydr. Res. 232*, 59−75.
9. Takakura, Y., and Kuwata, S. (2003) Purification, characterization, and molecular cloning of a pyranose oxidase from the fruit body of the basidiomycete *Tricholoma matsutake*, *Biosci. Biotechnol. Biochem. 67*, 2598−2607.
10. Leitner, C., Volc, J., and Haltrich, D. (2001) Purification and characterization of pyranose oxidase from the white rot fungus *Trametes multicolor*, *Appl. Environ. Microbiol. 67*, 3636−3644.
11. Freimund, S., Huwig, A., Giffhorn, F., and Köpper, S. (1998) Rare keto-aldoses from enzymatic oxidation: substrates and oxidation products of pyranose 2-oxidase, *Chem.−Eur. J. 4*, 2442−2455.
12. Albrecht, M., and Lengauer, T. (2003) Pyranose oxidase identified as member of the GMC oxidoreductase family, *Bioinformatics 19*, 1216−1220.
13. Cavener, D. R. (1992) GMC oxidoreductases, a newly defined family of homologous proteins with diverse catalytic activities, *J. Mol. Biol. 223*, 811−814.
14. Vrielink, A., Lloyd, L. F., and Blow, D. M. (1991) Crystal structure of cholesterol oxidase from *Brevibacterium sterolicum* refined at 1.8 Å resolution, *J. Mol. Biol. 219*, 533−554.
15. Yue, Q. K., Kass, I. J., Sampson, N. S., and Vrielink, A. (1999) Crystal structure determination of cholesterol oxidase from *Streptomyces* and structural characterization of key active site mutants, *Biochemistry 38*, 4277−4286.
16. Lario, P. I., Sampson, N., and Vrielink, A. (2003) Sub-atomic resolution crystal structure of cholesterol oxidase: what atomic resolution crystallography reveals about enzyme mechanism and the role of the FAD cofactor in redox activity, *J. Mol. Biol. 326*, 1635−1650.
17. Hecht, H. J., Kalisz, H. M., Hendle, J., Schmid, R. D., and Schomburg, D. (1993) Crystal structure of glucose oxidase from *Aspergillus niger* refined at 2.3 Å resolution, *J. Mol. Biol. 229*, 153−172.
18. Wohlfahrt, G., Witt, S., Hendle, J., Schomburg, D., Kalisz, K. M., and Hecht, H. J. (1999) 1.8 Å and 1.9 Å resolution structures of the *Penicillium amagasakiense* and *Aspergillus niger* glucose oxidases as basis for modelling substrate complexes, *Acta Crystallogr. D55*, 969−977.
19. Dreveny, I., Gruber, K., Glieder, A., Thompson, A., and Kratky, C. (2001) The hydroxynitrile lyase from almond: a lyase that looks like an oxidoreductase, *Structure 9*, 803−815.
20. Hallberg, B. M., Henriksson, G., Pettersson, G., and Divne, C. (2002) Crystal structure of the flavoprotein domain of the extracellular flavocytochrome cellobiose dehydrogenase, *J. Mol. Biol. 315*, 421−434.
21. Schulz, G. E., Schirmer, R. H., Sachsenheimer, W., and Pai, E. F. (1978) The structure of the flavoenzyme glutathione reductase, *Nature 273*, 120−124.
22. Dym, O., and Eisenberg, D. (2001) Sequence-structure analysis of FAD-containing proteins, *Protein Sci. 10*, 1712−1728.
23. Hendrickson, W. A., Horton, J. R., and LeMaster, D. M. (1990) Selenomethionyl proteins produced for analysis by multiwavelength anomalous diffraction (MAD): a vehicle for direct determination of three-dimensional structure, *EMBO J. 9*, 1665−1672.
24. Kabsch, W. (1993) Automatic processing of rotation diffraction data from crystals of initially unknown symmetry and cell constants, *J. Appl. Crystallogr. 26*, 795−800.
25. Schneider, T. R., and Sheldrick, G. M. (2002) Substructure solution with SHELXD, *Acta Crystallogr. D58*, 1772−1779.
26. Sheldrick, G. M. (2002) Macromolecular phasing with SHELXE, *Z. Kristallogr. 217*, 644−650.
27. Collaborative Computational Project, Number 4 (1994) The CCP4 Suite: Programs for Protein Crystallography, *Acta Crystallogr. D50*, 760−763.
28. Terwilliger, T. C. (2002) Automated structure solution, density modification and model building, *Acta Crystallogr. D58*, 1937−1940.
29. Bricogne, G., Vonrhein, C., Flensburg, C., Schiltz, M., and Paciorek, W. (2003) Generation, representation and flow of phase information in structure determination: recent developments in and around SHARP 2.0, *Acta Crystallogr. D59*, 2023−2030.
30. Jones, T. A., Zou, J. Y., Cowan, S. W., and Kjeldgaard, M. (1991) Improved methods for building protein models in electron density maps and location of errors in these models, *Acta Crystallogr. A47*, 110−119.
31. Brünger, A. T., Adams, P. D., Clore, G. M., DeLano, W. L., Gros, P., Grosse-Kunstleve, R. W., Jiang, J. S., Kuszewski, J., Nilges, M., Pannu, N. S., Read, R. J., Rice, L. M., Simonson, T., and Warren, G. L. (1998) Crystallography & NMR system: A new software suite for macromolecular structure determination, *Acta Crystallogr. D54*, 905−921.
32. Murshudov, G. N., Vagin, A. A., Lebedev, A., Wilson, K. S., and Dodson, E. J. (1999) Efficient anisotropic refinement of macromolecular structures using FFT, *Acta Crystallogr. D55*, 247−255.
33. van Aalten, D. M. F., Bywater, R., Findlay, J. B. C., Hendlich, M., Hooft, R. W., and Vriend, G. (1996) PRODRG, a program for generating molecular topologies and unique molecular descriptors from coordinates of small molecules, *J. Comput.-Aided Mol. Des. 10*, 255−262.
34. Perrakis, A., Morris, R. M., and Lamzin, V. S. (1999) Automated protein model building combined with iterative structure refinement, *Nat. Struct. Biol. 6*, 458−463.
35. Fenn, T. D., Ringe, D., and Petsko, G. A. (2003) POVSCRIPT+: a program for model and data visualization using persistance of vision ray-tracing, *J. Appl. Crystallogr. 36*, 944−947.
36. Sanner, M. F., Olson, A. J., and Spehner, J. C. (1996) Reduced surface: an efficient way to compute molecular surfaces, *Biopolymers 38*, 305−320.
37. Kroemer, M., and Schulz, G. E. (2002) The structure of L-rhamnulose-1-phosphate aldolase (class II) solved by low-resolution SIR phasing and 20-fold NCS-averaging, *Acta Crystallogr. D58*, 824−832.
38. Mewies, M., McIntire, W. S., and Scrutton, N. S. (1998) Covalent attachment of flavine adenine dinucleotide (FAD) and flavine mononucleotide (FMN) to enzymes: The current state of affairs, *Protein Sci. 7*, 7−20.
39. Halada, P., Leitner, C., Sedmera, P., Haltrich, D., and Volc, J. (2003) Identification of the covalent flavine adenine dinucleotide-binding region in pyranose 2-oxidase from *Trametes multicolor*, *Anal. Biochem. 314*, 235−242.
40. Altschul, S. F., Madden, T. L., Schäffer, A. A., Zhang, J., Zhang, Z., Miller, W., and Lipman, D. J. (1997) Gapped BLAST and PSI-BLAST: a new generation of protein database search programs, *Nucleic Acids Res. 25*, 3389−3402.
41. Nielsen, H., Engelbrecht, J., Brunak, S., and von Heijne, G. (1997) Identification of prokaryotic and eukaryotic signal peptides and prediction of their cleavage sites, *Protein Eng. 10*, 1−6.
42. Holm, L., and Sander, C. (1993) Protein structure comparison by alignment of distance matrices, *J. Mol. Biol. 233*, 123−138.
43. Schulz, G. E. (1992) Binding of nucleotides by proteins, *Curr. Opin. Struct. Biol. 2*, 61−67.
44. Meyer, E. A., Castellano, R. K., and Diederich, F. (2003) Interactions with aromatic rings in chemical and biological recognition, *Angew. Chem., Int. Ed. 42*, 1210−1250.
45. Fraaije, M. W., van den Heuvel, R. H., van Berkel, W. J., and Mattevi, A. (1999) Covalent flavinylation is essential for efficient redox catalysis in vanillyl-alcohol oxidase, *J. Biol. Chem. 274*, 35514−35520.
46. Hallberg, B. M., Henriksson, G., Pettersson, G., Vasella, A., and Divne, C. (2002) Mechanism of the reductive half-reaction in cellobiose dehydrogenase, *J. Biol. Chem. 278*, 7160−7166.
47. Meyer, E. W., and Schulz, G. E. (1997) Energy profile of maltooligosaccharide permeation through maltoporin as derived from the structure and from statistical analysis of saccharide-protein interactions, *Protein Sci. 6*, 1084−1091.

BI048609Q